

# KAPPA-MAXWELLIAN ELECTRONS AND BI-MAXWELLIAN PROTONS IN A TWO-FLUID MODEL FOR FAST SOLAR WIND

SOMAYEH TARAN,<sup>1</sup> HOSSEIN SAFARI,<sup>1</sup> AND FARHAD DAEI<sup>1</sup>

<sup>1</sup>*Department of Physics, Faculty of Science, University of Zanjan, P. O. Box 45195-313, Zanjan, Iran*

(Received 2018 August 24; Revised 2019 July 29; Accepted 2019 July 29)

## ABSTRACT

Modeling fast solar wind based on the kinetic theory is an important task for scientists. In this paper, we present a two-fluid model for fast solar wind with anisotropic Kappa-Maxwellian electrons and Bi-Maxwellian protons. In the simulation, the energy exchange between the plasma particles and low-frequency Alfvén waves is considered. A set of eleven coupled equations is derived by applying the zeroth- to fourth-order moments of the Vlasov equation and the modified electromagnetic Maxwell equations. A characteristic of the Kappa distribution (indicated by  $\kappa$  index) is explicit in the equation for the parallel component of the electron heat flux (parallel to the ambient magnetic field line) and differs from the equation derived for the proton heat flux due to the different nature of the distributions. Within the large  $\kappa$  index, the equations for the two-fluid model tend to the equations obtained by the Maxwellian distribution. Using an iterated Crank-Nicolson method, the coupled equations are numerically solved for the fast solar wind conditions. We show that at (0.3 - 1) AU from the Sun, the electron density, components of temperature, and components of heat flux follow the power-law behavior. We also showed that near the Earth, the flow speed (electron or proton) increases with decreasing  $\kappa$ . We concluded that applying the small  $\kappa$  index (the non-Maxwellian

distribution), the extraordinary nature of the solar atmosphere, with its temperature of several million kelvin temperature for electrons, has been captured.

*Keywords:* solar wind Sun: corona turbulence waves

## 1. INTRODUCTION

Cosmic rays and the huge volume of the solar wind plasma continually expose the Earth's atmosphere and its magnetic fields. The solar wind, flares, and coronal mass ejections show the interactions with the Earth's atmosphere and magnetic fields (e.g., geomagnetic disturbances), and may affect the space weather, communications, navigation systems, and astronauts (Chapman 1929; Parker 1958; Hartle & Sturrock 1968; Frank 1971; Perreault & Akasofu 1978; Young et al. 1982; Chappell et al. 1987; Gosling et al. 1991; Borovsky & Funsten 2003; Wheatland 2005; Gray et al. 2010; Chané et al. 2015; Cranmer et al. 2017; Raboonik et al. 2017; Farhang et al. 2018; Alipour et al. 2019).

Parker (1965) proposed the isothermal model for solar wind. In his model, the proton temperature anisotropy near the Earth plasma was not justified. After Parker (1965), several attempts have been made to investigate the behavior of the solar wind (Whang & Chang 1965; Durney 1971; Durney & Roberts 1971; Roberts & Soward 1972). Meyer-Vernet (2007) studied the solar wind from various perspectives, and Marsch (2006) considered wave-particle interactions in solar wind dynamics.

Observations revealed low values for the density of the solar wind. This wind mostly originates from the polar coronal holes during the solar minimum (Geiss et al. 1995; McComas et al. 2000, 2008). The particle distributions for fast solar wind deviate from the Maxwellian distribution (Lin 1980). Also, the solar wind plasma can be considered collisionless. Kulsrud (1983) presented a formulation for the collisional and collisionless plasma, which is useful for studying the solar wind.

In the kinetic study of the fast solar wind with non-Maxwellian distributions, the different sets of coupled equations partly agree with the solar wind observational data (e.g., Demars & Schunk 1990; Demars & Schunk 1991; Lie-Svendsen et al. 2001; Chandran et al. 2011). Snyder et al. (1997) developed a set of fluid momentum equations that describe the kinetic Landau damping for the plasma. They also considered the Coulomb collisions for the particles.

The particle distribution function is a key aspect of the study of the plasma wave-particle interactions and instabilities. For a homogeneous and isotropic plasma, the Maxwellian distribution determines the macroscopic parameters of the plasma in the thermal equilibrium and collisional condition

(Bittencourt 2004),

$$f_M = \frac{nm^{1/2}}{(2\pi k_B T)^{1/2}} \exp\left(-\frac{mv^2}{2k_B T}\right), \quad (1)$$

where  $n, m, k_B, T$ , and  $v$  represent the number density, particle mass, Boltzmann constant, temperature, and velocity, respectively. There are usually non-equilibrium conditions in the geophysical and space plasma, as the collisionless systems and the distributions of some high-energy particles deviate from the Maxwellian (Livadiotis 2017). With this objective in mind, the Kappa distribution function was proposed (e.g., Olbert 1968; Vasyliunas 1968; Pierrard et al. 2001):

$$f_\kappa = \frac{n}{(\pi\theta_\kappa^2)^{3/2}} \frac{\Gamma(\kappa+1)}{\Gamma(\kappa-\frac{1}{2})} \left(1 + \frac{v^2}{\kappa\theta_\kappa^2}\right)^{-(\kappa+1)}, \quad (2)$$

$$\theta_\kappa^2 = \left(1 - \frac{3}{2\kappa}\right) \left(\frac{2k_B T}{m}\right),$$

where  $\kappa$  is an index representing a deviation from the Maxwellian distribution and  $\Gamma$  indicates the gamma function. Within the limit of large  $\kappa$  ( $\kappa \rightarrow \infty$ ), the Kappa distribution tends to the Maxwellian one (Pierrard & Lazar 2010; Livadiotis & McComas 2013).

The Bi-Maxwellian distribution could explain the temperature anisotropy for the solar wind protons (Demars & Schunk 1990; Demars & Schunk 1991; Chandran et al. 2011). The tail (particles with high speeds and energies) of the electron distribution is well described by the Kappa or power-law distributions (Zouganelis et al. 2004). The electron distribution can be classified into two categories: thermal core and suprathermal halo population (Vasyliunas 1968; Pierrard et al. 2001).

Observations showed that the wave turbulence has a significant effect on the propagation of the solar wind (Coleman 1968). This could be responsible for the heating and acceleration of the solar wind.

Morton et al. (2015) verified the existence of the Alfvén wave in the coronal open magnetic field regions as one of the reasons for the acceleration of the solar wind. The *Voyager's* observations gave evidence for the presence of the Alfvén wave fluctuations in the solar wind up to 8 AU from the Sun (Roberts et al. 1987; Bruno & Carbone 2005). Landau damping is an important mechanism for the Alfvén wave damping in collisionless plasma (Lysak & Lotko 1996; TenBarge et al. 2013). In this

mechanism, the oscillatory modes for plasma damp in the collisionless regime of a plasma. In non-Maxwellian distributions with suprathermal particles, the probability of Landau damping has a high value (Basu 2009; Pierrard & Lazar 2010; Rudakov et al. 2011; Qureshi et al. 2014). Sharma et al. (2016) suggested the heating of particles in the inhomogeneous plasma related to the kinetic Alfvén wave (KAW) Landau damping.

The existence of anisotropic temperatures in plasma is a major reason for the application of the non-Maxwellian distribution for the particles. The appearance and growth of instabilities are the results of deviation from the isotropy temperature (Shaaban et al. 2017).

Hellinger et al. (2006) studied the oblique, mirror, and oblique firehose instabilities using the WIND/SWE observational values and the temperature ratio (the ratio of the perpendicular component of temperature to the parallel component). Kasper et al. (2006) showed that the mirror and cyclotron instabilities control the anisotropy for  $T_{\perp p}/T_{\parallel p} > 1$ , and that the firehose instability controls the anisotropy for  $T_{\perp p}/T_{\parallel p} < 1$ . The several instability mechanisms and wave turbulences in the solar corona and solar wind have been widely investigated (e.g., Chandran 2018; Shoda et al. 2018a,b).

Chandran et al. (2011) proposed a 1D, two-fluid model for the solar wind. They considered Maxwellian and Bi-Maxwellian distribution functions for the electrons and protons, respectively. They derived a set of coupled equations for the protons in parallel and perpendicular to the ambient magnetic field direction. The equations for quantities related to the system of electrons are also coupled with equations corresponding to the system of protons. They considered the low-frequency Alfvén wave in the wave-particle interactions and calculated heating rates of protons in two directions and the total heating rate of electrons. By applying the moments of the Vlasov equation, they derived a set of eight coupled equations. The set of equations in the solar wind conditions was solved with the Hu et al. (1997) method.

In this paper, we extend the Chandran et al. (2011) model for the fast solar wind in the framework constructed by Snyder et al. (1997) by applying the Kappa-Maxwellian distribution for electrons instead of the Maxwellian distribution. Consequently, we obtain separate equations for the components of electron temperature and heat flux. Using the zeroth- to fourth-order moments of the Vlasov

equation, we derive a set of eleven coupled equations (instead of the 8 coupled equations given by Chandran et al. (2011)).

We solved the equations by applying the Iterated Crank-Nicolson (ICN) numerical method. Discretizing equations with the ICN method has second-order accuracy in space and time, which offers accurate computational results.

The details of the derivation of the set of the coupled equations for the present two-fluid model are given in Section 2. The instabilities driven by temperature anisotropy are presented in Section 3. Calculations of the heating rate for electrons and protons are provided in Section 4. In Section 5, we present a numerical method for solving the 11 coupled equations. Numerical results are presented in Section 6, and they are compared with observations and previous studies. A conclusion is given in Section 7.

## 2. EQUATIONS OF THE TWO-FLUID SOLAR WIND MODEL

The formulation of the present model for the collisionless magnetohydrodynamics (MHD) is based on Kulsrud (1983). For this purpose, a thin open magnetic flux tube originating from a solar coronal hole along with the solar radii is considered. A cylindrical coordinate with the z-axis along the magnetic field is used (Figure 1). The Sun's rotation is not considered in the calculations.

The fundamental variables are as follows: the mass density  $\rho$ , the fluid velocity  $\mathbf{U} = \mathbf{v}_E + u_{\parallel}\hat{\mathbf{b}}$  (which is the same for electrons and protons), the magnetic field  $\mathbf{B}$ , the proton distribution function  $f_p$ , the electron distribution function  $f_e$ , and the parallel component of the electric field  $E_{\parallel} = \hat{\mathbf{b}} \cdot \mathbf{E}$  ( $\hat{\mathbf{b}} = \mathbf{B}/B$  is a unit vector along the magnetic field). After that, we used the notation used by Chandran et al. (2011).

In Kulsrud's formulation, the Vlasov equation is given by (Kulsrud 1983; Snyder et al. 1997)

$$\frac{\partial}{\partial t}(f_s B) + \nabla \cdot [f_s B(v_{\parallel}\hat{\mathbf{b}} + \mathbf{v}_E)] + \frac{\partial}{\partial v_{\parallel}} \times [f_s B(-\hat{\mathbf{b}} \cdot \frac{D\mathbf{v}_E}{Dt} - \mu\hat{\mathbf{b}} \cdot \nabla B + \frac{e_s E_{\parallel}}{m_s})] = 0, \quad (3)$$

where  $s$  indicates particle species ( $p$  for proton and  $e$  for electron),  $f_s$  is the particle distribution function,  $m_s$  and  $e_s$  are the mass and charge, and  $\mathbf{v}$  is the velocity of the particle ( $v_{\parallel} = \hat{\mathbf{b}} \cdot \mathbf{v}$ ,  $\mathbf{v}_E = c(\mathbf{E} \times \mathbf{B})/B^2$ ,  $\mu = v_{\perp}^2/2B$ ).

The total derivative is defined by  $D/Dt = \partial/\partial t + (v_{\parallel}\hat{\mathbf{b}} + \mathbf{v}_E) \cdot \nabla$ . The distribution function ( $f_s$ ) is a function of position  $\mathbf{r}$  (heliocentric distance in the solar wind model), time  $t$ , magnetic moment  $\mu$ , and the parallel component of velocity  $v_{\parallel}$ .

The collisionless MHD equations can be derived by evaluating different orders of the velocity moments (Equation 3) and the modified electromagnetic Maxwell equations. Given the limit of low Alfvén speed ( $v_A^2 \leq c^2$ ), the continuity and momentum equations are given by (Snyder et al. 1997),

$$\frac{\partial \rho}{\partial t} + \nabla \cdot (\rho \mathbf{U}) = 0, \quad (4)$$

$$\rho \left( \frac{\partial \mathbf{U}}{\partial t} + \mathbf{U} \cdot \nabla \mathbf{U} \right) = \frac{(\nabla \times \mathbf{B}) \times \mathbf{B}}{4\pi} - \nabla \cdot \mathbf{P} - \frac{GM_{\odot}\rho}{r^2} \hat{\mathbf{b}} - \frac{1}{2} \frac{\partial E_W}{\partial r} \hat{\mathbf{b}}. \quad (5)$$

The third and fourth terms on the right side of Equation (5) are the gravitational acceleration and the Alfvén wave pressure force, respectively. The pressure tensor  $\mathbf{P}$  can be written as (Goedbloed et al. 2004),

$$\mathbf{P} = \sum_s p_{\perp s} (\mathbf{I} - \hat{\mathbf{b}}\hat{\mathbf{b}}) + \sum_s p_{\parallel s} \hat{\mathbf{b}}\hat{\mathbf{b}}, \quad (6)$$

where  $\mathbf{I}$  is an unit dyadic. The parallel and perpendicular components of the pressure tensor are given by

$$p_{\perp s} := \frac{m_s}{2} \int f_s v_{\perp}^2 d^3 v, \quad (7)$$

$$p_{\parallel s} := m_s \int f_s (v_{\parallel} - U_{\parallel})^2 d^3 v. \quad (8)$$

The number density is defined as

$$n_s := \int f_s d^3 v. \quad (9)$$

The induction equation is introduced by

$$\frac{\partial \mathbf{B}}{\partial t} = \nabla \times (\mathbf{U} \times \mathbf{B}). \quad (10)$$

In the lowest order in  $1/e$ , the electrostatic Poisson equation for charges and number densities is reduced to the condition,  $\sum_s e_s n_s = 0$  (Kulsrud 1983). Furthermore, we assume  $n = n_p = n_e$ . The

electron contribution to mass density is not considered, and the total mass density is  $\rho = nm_p$ . The perpendicular pressure  $p_{\perp s}$  satisfies (Snyder et al. 1997; Sharma et al. 2006; Chandran et al. 2011),

$$\rho B \frac{d}{dt} \left( \frac{p_{\perp s}}{\rho B} \right) = -\nabla \cdot (q_{\perp s} \hat{\mathbf{b}}) - q_{\perp s} \nabla \cdot \hat{\mathbf{b}} + \frac{\nu_s}{3} (p_{\parallel s} - p_{\perp s}), \quad (11)$$

where  $\nu_s$  is the Coulomb collision frequency for the energy exchange between particles. Moreover, the parallel component of pressure  $p_{\parallel s}$  obeys

$$\frac{\rho^3}{2B^2} \frac{d}{dt} \left( \frac{B^2 p_{\parallel s}}{\rho^3} \right) = -\nabla \cdot (q_{\parallel s} \hat{\mathbf{b}}) + q_{\perp s} \nabla \cdot \hat{\mathbf{b}} + \frac{\nu_s}{3} (p_{\perp s} - p_{\parallel s}), \quad (12)$$

where the perpendicular and parallel components of the heat flux are defined by

$$q_{\perp s} := m_s \int f_s \mu B (v_{\parallel} - U_{\parallel}) d^3 v, \quad (13)$$

$$q_{\parallel s} := \frac{m_s}{2} \int f_s (v_{\parallel} - U_{\parallel})^3 d^3 v. \quad (14)$$

The perpendicular heat flux  $q_{\perp s}$  is given by

$$\begin{aligned} \rho^2 \frac{d}{dt} \left( \frac{q_{\perp s}}{\rho^2} \right) + \nu_s q_{\perp s} = & -\nabla \cdot (r_{\perp\perp} \hat{\mathbf{b}}) + \frac{p_{\perp s}}{\rho} \hat{\mathbf{b}} \cdot \nabla p_{\parallel s} \\ & + \left[ \frac{p_{\perp s} (p_{\parallel s} - p_{\perp s})}{\rho} + r_{\perp\perp} - r_{\parallel\perp} \right] \nabla \cdot \hat{\mathbf{b}}, \end{aligned} \quad (15)$$

and for  $q_{\parallel s}$  is

$$\begin{aligned} \frac{\rho^4}{B^3} \frac{d}{dt} \left( \frac{B^3 q_{\parallel s}}{\rho^4} \right) + \nu_s q_{\parallel s} = & -\frac{1}{2} \nabla \cdot (r_{\parallel\parallel} \hat{\mathbf{b}}) + \frac{3p_{\parallel s}}{2\rho} \hat{\mathbf{b}} \cdot \nabla p_{\parallel s} \\ & + \frac{3}{2} \left[ \frac{p_{\parallel s} (p_{\parallel s} - p_{\perp s})}{\rho} + r_{\perp\parallel} \right] \nabla \cdot \hat{\mathbf{b}}. \end{aligned} \quad (16)$$

The fourth-order moments of the Vlasov equation ( $r_{\perp\perp}, r_{\parallel\perp}, r_{\parallel\parallel}$ ) are introduced by

$$r_{\perp\perp} := m_s \int f_s \mu^2 B^2 d^3 v, \quad (17)$$

$$r_{\parallel\perp} := m_s \int f_s \mu B (v_{\parallel} - U_{\parallel})^2 d^3 v, \quad (18)$$

$$r_{\parallel\parallel} := m_s \int f_s (v_{\parallel} - U_{\parallel})^4 d^3 v. \quad (19)$$

We consider the Kappa-Maxwellian distribution function for the electrons as follows:

$$f_e = f_{\kappa M}(v_{\parallel}, v_{\perp}) = \frac{n}{\pi^{3/2} \theta_{\perp e}^2 \theta_{\parallel e}} \frac{\Gamma(\kappa + 1)}{\kappa^{3/2} \Gamma(\kappa - \frac{1}{2})} \left( 1 + \frac{(v_{\parallel e} - U_{\parallel e})^2}{\kappa \theta_{\parallel e}^2} \right)^{-\kappa} \exp \left( -\frac{v_{\perp e}^2}{\theta_{\perp e}^2} \right), \quad (20)$$



where the parallel and perpendicular components of the thermal velocities are defined as

$$\theta_{\parallel e} = \left( \frac{2\kappa - 3}{\kappa} \right)^{\frac{1}{2}} \left( \frac{k_B T_{\parallel e}}{m_e} \right)^{\frac{1}{2}}, \quad \theta_{\perp e} = \left( \frac{2k_B T_{\perp e}}{m_e} \right)^{\frac{1}{2}}.$$

For the Kappa distribution, the spectral index  $\kappa$  is a free parameter and varies from 1.5 to infinity (Pierrard & Lazar 2010). The Bi-Maxwellian distribution function for protons is introduced by

$$f_p = f_{BM} = \frac{nm_p^{3/2}}{(2\pi k_B)^{3/2} T_{\perp p} T_{\parallel p}^{1/2}} \exp \left( -\frac{m_p \mu_p B}{k_B T_{\perp p}} - \frac{m_p (v_{\parallel p} - U_{\parallel p})^2}{2k_B T_{\parallel p}} \right). \quad (21)$$

In the reminder of this section, we explore the explicit effects of the electron and proton distribution functions on the quantities of the system of the two-fluid model. The relation between the fourth-order moments,  $r_{\perp\perp}$ ,  $r_{\perp\parallel}$ ,  $r_{\parallel\parallel}$  (Equations 17, 18, and 19) and main quantities ( $n$ ,  $p$ ,  $T$ ,  $U$ , etc.), are derived.

Suppose a straight flux tube with a magnetic field along the solar radius  $r$ . Then we have

$$\hat{\mathbf{b}} \cdot \nabla \equiv \frac{\partial}{\partial r}, \quad \nabla \cdot \hat{\mathbf{b}} = \frac{1}{a} \frac{\partial a}{\partial r}, \quad (22)$$

where  $a$  is the cross section of the flux tube (Kopp & Holzer 1976). Additionally, we assume all the quantities are the function of solar radii ( $r$ ) (along with the axis of the flux tube) and are considered as axially symmetric (independent of  $\phi$  in cylindrical coordinate).

The continuity, momentum, and pressure equations, which are the same for both electrons and protons, are derived from the zeroth- to second-order moments of the Vlasov equation. Owing to the different nature of the distributions for electrons and protons, the equations for the electron heat flux are different from the proton heat flux.

The set of variables depending on the time ( $t$ ) and radial coordinate ( $r$ ) comprises the following: number density  $n$  (proton or electron), outflow velocity  $U$  (proton or electron), perpendicular and parallel electron temperatures  $T_{\perp e}$  and  $T_{\parallel e}$ , perpendicular and parallel proton temperatures  $T_{\perp p}$  and  $T_{\parallel p}$ , electron heat fluxes  $q_{\perp e}$  and  $q_{\parallel e}$ , proton heat fluxes  $q_{\perp p}$  and  $q_{\parallel p}$ , and wave energy  $E_W$ .

Using Equation (22), the continuity equation (Equation 4) gives

$$\frac{dn}{dt} = -\frac{n}{a} \frac{\partial}{\partial r} (aU), \quad n = n_p = n_e. \quad (23)$$

Substituting the pressure tensor from Equation (6) with the momentum equation (Equation 5), and after some algebra manipulation, one finds

$$\frac{dU}{dt} = -\frac{k_B}{\rho} \frac{\partial}{\partial r} (n(T_{\parallel e} + T_{\parallel p})) + \frac{k_B[(T_{\perp p} - T_{\parallel p}) + (T_{\perp e} - T_{\parallel e})]}{m_p a} \frac{\partial a}{\partial r} - \frac{GM_\odot}{r^2} - \frac{1}{2\rho} \frac{\partial E_W}{\partial r}. \quad (24)$$

By calculating the fourth-order moments (Equations 17 - 19)) according to the related distribution function, we find parallel and perpendicular electron heat fluxes:

$$\rho^2 \frac{d}{dt} \left( \frac{q_{\perp e}}{\rho^2} \right) + \nu_e q_{\perp e} = -\frac{nk_B^2 T_{\parallel e}}{m_e} \frac{\partial T_{\perp e}}{\partial r} + \frac{nk_B^2 T_{\perp e} (T_{\perp e} - T_{\parallel e})}{m_e a} \frac{\partial a}{\partial r}, \quad (25)$$

$$\begin{aligned} \frac{\rho^4}{B^3} \frac{d}{dt} \left( \frac{B^3 q_{\parallel e}}{\rho^4} \right) + \nu_e q_{\parallel e} = & + \frac{3n^2 k_B^2 T_{\parallel e}^2}{(5-2\kappa)\rho} \frac{1}{a} \frac{\partial a}{\partial r} \\ & + \frac{3(2\kappa-1)}{2(5-2\kappa)} \frac{n^2 k_B^2 T_{\parallel e}}{\rho} \frac{\partial T_{\parallel e}}{\partial r} + \frac{3}{(5-2\kappa)} \frac{nk_B^2 T_{\parallel e}^2}{\rho} \frac{\partial n}{\partial r}. \end{aligned} \quad (26)$$

The proton heat flux equations are given by (e.g., Chandran et al. 2011)

$$\rho^2 \frac{d}{dt} \left( \frac{q_{\perp p}}{\rho^2} \right) + \nu_p q_{\perp p} = -\frac{nk_B^2 T_{\parallel p}}{m_p} \frac{\partial T_{\perp p}}{\partial r} + \frac{nk_B^2 T_{\perp p} (T_{\perp p} - T_{\parallel p})}{m_p a} \frac{\partial a}{\partial r}, \quad (27)$$

$$\frac{n^4}{B^3} \frac{d}{dt} \left( \frac{B^3 q_{\parallel p}}{n^4} \right) + \nu_p q_{\parallel p} = -\frac{3nk_B^2 T_{\parallel p}}{2m_p} \frac{\partial T_{\parallel p}}{\partial r}. \quad (28)$$

Now, we use the temperatures instead of the pressures in the equations for both electrons and protons. This can be done by substituting  $p_{\perp} = nk_B T_{\perp}$  and  $p_{\parallel} = nk_B T_{\parallel}$  in Equations (11) and (12) for electron temperatures,

$$\begin{aligned} Bnk_B \frac{d}{dt} \left( \frac{T_{\perp e}}{B} \right) = & Q_{\perp e} - \frac{1}{a^2} \frac{\partial}{\partial r} (a^2 q_{\perp e}) + \frac{1}{3} \nu_e nk_B (T_{\parallel e} - T_{\perp e}) \\ & + 2\nu_{ep} nk_B (T_p - T_{\perp e}), \end{aligned} \quad (29)$$

$$\begin{aligned} \frac{n^3 k_B}{2B^2} \frac{d}{dt} \left( \frac{B^2 T_{\parallel e}}{n^2} \right) = & Q_{\parallel e} - \frac{1}{a} \frac{\partial}{\partial r} (a q_{\parallel e}) + \frac{q_{\perp e}}{a} \frac{\partial a}{\partial r} \\ & + \frac{1}{3} \nu_e nk_B (T_{\perp e} - T_{\parallel e}) + \nu_{ep} nk_B (T_p - T_{\parallel e}). \end{aligned} \quad (30)$$

The parallel and perpendicular components of the proton temperature obey the following equations:

$$Bnk_B \frac{d}{dt} \left( \frac{T_{\perp p}}{B} \right) = Q_{\perp p} - \frac{1}{a^2} \frac{\partial}{\partial r} (a^2 q_{\perp p}) + \frac{1}{3} \nu_p n k_B (T_{\parallel p} - T_{\perp p}) + 2\nu_{pe} n k_B (T_e - T_{\perp p}), \quad (31)$$

$$\frac{n^3 k_B}{2B^2} \frac{d}{dt} \left( \frac{B^2 T_{\parallel p}}{n^2} \right) = Q_{\parallel p} - \frac{1}{a} \frac{\partial}{\partial r} (a q_{\parallel p}) + \frac{q_{\perp p}}{a} \frac{\partial a}{\partial r} + \frac{1}{3} \nu_p n k_B (T_{\perp p} - T_{\parallel p}) + \nu_{pe} n k_B (T_e - T_{\parallel p}). \quad (32)$$

In Equations (29)-(32), the quantities  $(Q_{\perp e}, Q_{\parallel e})$  and  $(Q_{\perp p}, Q_{\parallel p})$  are the heating rates per unit volume for electrons and protons, respectively. In Section 4, the details of heating rates are given.

Finally, the last equation for wave energy  $E_W$  is given by (Dewar 1970)

$$\frac{\partial E_W}{\partial t} + \frac{1}{a} \frac{\partial}{\partial r} [a(U + v_A)E_W] + \frac{E_W}{2a} \frac{\partial}{\partial r} (aU) = -Q, \quad (33)$$

where the Alfvén speed is  $v_A = \frac{B}{\sqrt{4\pi\rho}}$ , the total heating rate is  $Q = Q_{\perp e} + Q_{\parallel e} + Q_{\perp p} + Q_{\parallel p}$ , and the total temperature is defined as  $T = \frac{T_{\parallel} + 2T_{\perp}}{3}$ . Using Equations (24) and (29)-(33), the total energy equation is obtained:

$$\frac{\partial E_{\text{tot}}}{\partial t} + \frac{1}{a} \frac{\partial}{\partial r} (a F_{\text{tot}}) = 0, \quad (34)$$

where  $E_{\text{tot}}$  is the total energy density and is defined as

$$E_{\text{tot}} = \frac{\rho U^2}{2} - \frac{GM_{\odot}\rho}{r} + nk_B(T_{\perp e} + \frac{T_{\parallel e}}{2} + T_{\perp p} + \frac{T_{\parallel p}}{2}) + E_W, \quad (35)$$

and  $F_{\text{tot}}$  is the total energy flux and is defined as

$$F_{\text{tot}} = \frac{\rho U^3}{2} - \frac{UGM_{\odot}\rho}{r} + Unk_B(T_{\perp e} + \frac{3T_{\parallel e}}{2} + T_{\perp p} + \frac{3T_{\parallel p}}{2}) + q_{\text{total}} + (\frac{3U}{2} + v_A)E_W, \quad (36)$$

where  $q_{\text{tot}} = q_{\perp e} + q_{\perp p} + q_{\parallel e} + q_{\parallel p}$ . In Equation (36), the first, second, third, and last terms are the kinetic energy flux, gravitational potential energy, enthalpy flux, and Alfvén wave enthalpy flux, respectively.

In the steady state,  $\frac{\partial E_{\text{tot}}}{\partial t} = 0$ , the total energy flux is conserved and constant along the flux tube (solar radius).

### 2.1. The Limit of Large $\kappa$

Generally, observations of the space plasma showed that the tail of the distribution is likely to be the power-law function. It is important to use the Kappa distribution as a non-Maxwellian distribution for such plasmas. The Kappa distribution approach to the Maxwellian distribution for large  $\kappa$  index ( $\kappa$  tends to  $\infty$ ) and for finite  $\kappa$  differs from the Maxwellian. Therefore, we expect that, in the limit of large  $\kappa$ , the set of equations derived in the presence of the Kappa-Maxwellian approach to the Bi-Maxwellian set.

The parallel component of the electron heat flux (Equation 26) with the Kappa-Maxwellian distribution has an explicit dependency on the  $\kappa$  index. In the limit of the large  $\kappa$ , and by setting  $\rho = m_p n$ , the equation for the parallel electron heat flux Equation (26) can be rewritten as

$$\frac{n^4}{B^3} \frac{d}{dt} \left( \frac{B^3 q_{\parallel e}}{n^4} \right) + \nu_e q_{\parallel e} = - \frac{3n^2 k_B^2 T_{\parallel e}}{2\rho} \frac{\partial T_{\parallel e}}{\partial r}, \quad (37)$$

Equation (37) has the same form for the parallel heat flux obtained for the Bi-Maxwellian distribution function. Other quantities are coupled with the electron heat flux and depend on the  $\kappa$  index.

## 3. INSTABILITIES DRIVEN BY TEMPERATURE ANISOTROPY

Anisotropic behavior of the temperature of particles (electron and proton) leads to plasma instabilities (Gary & Wang 1996; Shaaban et al. 2017). The proton and electron temperature anisotropy ratios are defined by  $R_p = T_{\perp p}/T_{\parallel p}$  and  $R_e = T_{\perp e}/T_{\parallel e}$ , respectively. Observations show that for plasma stability, these ratios should remain in the specific ranges. The oblique firehose and mirror instabilities restrict the  $R_p$  for the lower and upper limits for protons. Also, mirror and Whistler instabilities control the lower and upper limits of the  $R_e$  for electrons (Kalman et al. 1968; Gary & Wang 1996; Kasper et al. 2002; Gary & Karimabadi 2006; Hellinger et al. 2006; Bale et al. 2009). The values of both  $R_p$  and  $R_e$  are related to the plasma beta parameter ( $\beta_{\parallel}$ ). In the case of  $\gamma_{max} \leq 10^{-3} \Omega_p$ , where  $\gamma_{max}$  is the maximum growth rate of instabilities and  $\Omega_p$  is the proton cyclotron frequency, the relations for instabilities (mirror and oblique firehose) of protons temperature anisotropy are given by

$$R_{p,m} = 1 + 0.77(\beta_{\parallel p} + 0.016)^{-0.76}, \quad R_{p,f} = 1 - 1.4(\beta_{\parallel p} + 0.11)^{-1}, \quad (38)$$

in which  $\beta_{\parallel p} = \frac{8\pi n k_B T_{\parallel p}}{B^2}$  (Hellinger et al. 2006). The instabilities (Whistler and mirror) for electrons temperature anisotropy are given by

$$R_{e,w} = 1 + 0.15\beta_{\parallel e}^{-0.56}, \quad R_{e,m} = 1 + 0.53\beta_{\parallel e}^{-0.64}, \quad (39)$$

where  $\beta_{\parallel e} = \frac{8\pi n k_B T_{\parallel e}}{B^2}$  (Gary & Karimabadi 2006).

Following Chandran et al. (2011), we insert the temperature-driven anisotropy effects in terms of  $\nu_{\text{inst}}$  for protons as follows:

$$\nu_{p,\text{inst}} = \nu_0 \exp\left(\frac{12(R_p - R_{p,m})}{R_{p,m}}\right) + \nu_0 \exp\left(\frac{12(\bar{R}_{p,f} - R_p)}{\bar{R}_{p,f}}\right), \quad \bar{R}_{p,f} = \max(R_{p,f}, 10^{-6}), \quad (40)$$

and  $\nu_{e,\text{inst}}$  for electrons is as follows:

$$\nu_{e,\text{inst}} = \nu_0 \exp\left(\frac{12(R_e - R_{e,w})}{R_{e,w}}\right) + \nu_0 \exp\left(\frac{12(R_{e,m} - R_e)}{R_{e,m}}\right), \quad (41)$$

where  $\nu_0 = 0.02\sqrt{GM_{\odot}/R_{\odot}^3}$ . Finally,  $\nu_p$  and  $\nu_e$  are defined as

$$\nu_p = \nu_{pp} + \nu_{p,\text{inst}}, \quad \nu_e = \nu_{ee} + \nu_{e,\text{inst}}, \quad (42)$$

in which  $\nu_{pp}$  and  $\nu_{ee}$  are the proton-proton and electron-electron Coulomb collision frequency (Schunk 1975).

#### 4. HEATING RATES

The nature of the turbulence dissipation of the solar wind is not yet to be well understood, but observations and analytical calculations have verified the Alfvénic turbulence effects in the damping mechanisms (e.g. Jiang et al. 2009; Chen et al. 2010; Vranjes & Poedts 2010; Salem et al. 2012; TenBarge et al. 2013; Meng et al. 2015; Wu et al. 2016; Schreiner & Saur 2017).

For the plasma with spatial scales much larger than the particle's mean free path, the MHD approach provides a suitable description of the propagation without damping the fast, intermediate (Alfvén), and slow modes. Hence, undamped plasma waves cascade to the small scales.

In general, an Alfvén wave is a type of MHD waves in which the ions vibrate due to the disturbing of the magnetic field lines in a magnetized plasma. Both transverse and longitudinal Alfvén waves

have been detected (e.g., [Hollweg 1981](#); [Amagishi 1986](#)). In transverse Alfvén waves (shear Alfvén wave) both the disturbance of the magnetic field and the motion of ions are in the same direction and perpendicular to the direction of the wave vector (propagation direction) ([Alfvén & Lindblad 1947](#); [Cramer 2011](#); [Priest 2014](#); [Esmaeili et al. 2016](#)).

The Alfvén modes remain undamped until the structures of the plasma reach the size of the proton gyroradius. The KAW fluctuations appear in the turbulence cascades of Alfvén waves and move their fluid scale to the smaller structures (kinetic scale) ([Zhao et al. 2011](#); [Gershman et al. 2017](#)), thus creating non-thermal particles. For more details, see [Howes \(2008, 2015\)](#), [Howes et al. \(2011\)](#).

Depending on the dissipation mechanism, the total heating rate  $Q$  is divided between the electrons ( $Q_{\perp e}, Q_{\parallel e}$ ) and protons ( $Q_{\perp p}, Q_{\parallel p}$ ). The contribution of each species to the total heating rate could be calculated by a numerical solution of the dispersion relation for the Alfvén wave.

By linearizing the Maxwell equations, the following dispersion relation is given in the Fourier space  $(\omega, k)$  (e.g., [Quataert 1998](#); [Stix 1992](#)) as,

$$\mathbf{k} \times (\mathbf{k} \times \mathbf{E}) + \frac{\omega^2}{c^2} \epsilon \cdot \mathbf{E} = \mathbf{0}, \quad (43)$$

where  $E$ ,  $\epsilon$ ,  $k$ ,  $\omega$ , and  $c$  represent the electric field perturbation, dielectric tensor, wave vector, wave frequency, and light speed, respectively. The dielectric tensor is related to the susceptibility tensor by

$$\epsilon_{ij} = \delta_{ij} + \sum_s \chi_{ij}^s. \quad (44)$$

The components of the susceptibility tensor are computed by [Cattaert et al. \(2007\)](#). To study the Alfvén wave and KAW interactions with plasma particles, we consider two ranges:  $k_{\perp} \rho_p \sim 1$  (for protons) and  $k_{\perp} \rho_p \gg 1$  (for electrons). The parallel wavenumber ( $k_{\parallel}$ ) is obtained by the critical balance condition ([Goldreich & Sridhar 1995](#); [Cho & Vishniac 2000](#); [Maron & Goldreich 2001](#); [TenBarge & Howes 2012](#)). [Stix \(1992\)](#) calculate particle damping rates. Following [Chandran et al. \(2011\)](#), we calculate the parallel and perpendicular components of the electron and proton heating

rates as

$$Q_{\parallel e} = \frac{(1 + \gamma_{\parallel e} t_c) Q}{1 + \gamma_{\text{tot}} t_c}, \quad (45)$$

$$Q_{\perp e} = \frac{\gamma_{\perp e} t_c Q}{1 + \gamma_{\text{tot}} t_c}, \quad (46)$$

$$Q_{\parallel p} = \frac{\gamma_{\parallel p} t_c Q}{1 + \gamma_{\text{tot}} t_c}, \quad (47)$$

$$Q_{\perp p} = \frac{\gamma_{\perp p} t_c Q}{1 + \gamma_{\text{tot}} t_c}, \quad (48)$$

where  $t_c = \rho \delta v_p^2 / Q$  is the time that the energy cascades at the scale  $k_{\perp} \rho_p = 1$ .  $\delta v_p$  is the root mean square (rms) of the Alfvén and/or KAW fluctuations.

Total heating rate per unit volume is introduced by [Chandran et al. \(2011\)](#) as

$$Q = \frac{c_d \rho z_{\text{rms}}^- (z_{\text{rms}}^+)^2}{4 L_{\perp}}, \quad (49)$$

where  $c_d = 0.75$  is a dimensionless number, and  $z_{\text{rms}}^-$  and  $z_{\text{rms}}^+$  are the Elsasser variables that satisfy the following equations:

$$E_W = \frac{\rho (z_{\text{rms}}^+)^2}{4}, \quad (50)$$

$$z_{\text{rms}}^- = \frac{L_{\perp} (U + v_A)}{v_A} \left| \frac{\partial v_A}{\partial r} \right|. \quad (51)$$

$L_{\perp}$  is the correlation length scale due to the Alfvénic fluctuations.

## 5. NUMERICAL METHOD

In this study, we build a system of coupled nonlinear partial differential equations (Equations 23-33) in the following general form:

$$\frac{\partial \psi(x, t)}{\partial t} = \mathcal{L}(\psi(x, t)), \quad (52)$$

where  $\psi(x, t)$  and  $\mathcal{L}$  are the vector of quantities and partial differential operator, respectively. We convert Equation (52) to the Euler frame, and then discretize the equation(s) using the finite difference method in the spatial dimension by the mid-point approximation and forward in time as ([Recktenwald](#)

2004; Meis & Marcowitz 2012; Thomas 2013),

$$\begin{aligned}\frac{\partial\psi(x,t)}{\partial x} &\approx \frac{\psi_{i+1}^j - \psi_{i-1}^j}{x_{i+1} - x_{i-1}} \\ \frac{\partial\psi(x,t)}{\partial t} &\approx \frac{\psi_i^{j+1} - \psi_i^j}{t_{j+1} - t_j}\end{aligned}\tag{53}$$

where the  $i$  and  $j$  indices represent the spatial and time steps, respectively. To solve the system of partial differential equations (Equations 24-33), we implement the ICN method (Leiler & Rezzolla 2006), which is based on the prediction, correction, and averaging of the quantities.

The Crank-Nicolson method has second-order accuracy in both time and space (Teukolsky 2000). In the method, two iterations are used to solve the Equation (52). These two steps produce the iterative equations

$$^{(1)}\tilde{\psi}_i^{n+1} = \psi_i^n + \Delta t \mathcal{L}(\psi_m^n),\tag{54}$$

$$^{(1)}\bar{\psi}_i^{n+1/2} \equiv \frac{1}{2} \left( ^{(1)}\tilde{\psi}_i^{n+1} + \psi_i^n \right),\tag{55}$$

$$^{(2)}\tilde{\psi}_i^{n+1} = \psi_i^n + \Delta t \mathcal{L}(^{(1)}\bar{\psi}_m^{n+1/2}),\tag{56}$$

$$^{(2)}\bar{\psi}_i^{n+1/2} \equiv \frac{1}{2} \left( ^{(2)}\tilde{\psi}_i^{n+1} + \psi_i^n \right),\tag{57}$$

$$\psi_i^{n+1} = \psi_i^n + \Delta t \mathcal{L}(^{(2)}\bar{\psi}_m^{n+1/2}),\tag{58}$$

where  $\tilde{\psi}$  and  $\bar{\psi}$  are the predicted-corrected and averaged functions, respectively. The value of the index  $m$  depends on the order of operator  $\mathcal{L}$  and second-order accuracy. For the first-order spatial derivative, we choose  $m = i \pm 1$ . Each time step is adopted considering the stability condition of the ICN method.

To avoid the non-physical oscillations and also to increase stability in ICN outputs, we add the artificial diffusion term as  $-D \frac{\partial^2 \psi}{\partial x^2}$  to the right sides of equations, in which  $D$  is a positive constant. Empirically, we found that (a) the value of the diffusion constant need not all be equal for all equations; (b) for small values of the diffusion constants ( $0 \leq D \leq 5$ ), the computational algorithm remains stable; (c) the diffusion terms for some quantities (e.g., fluid velocity, temperatures) are more important than those for others (e.g., number density).



We use a logarithmic grid in the space ( $r$ ) with a growing size by increasing the distance from the origin due to rapid changes in the physical quantities near the Sun. The parameter  $r_i$  ( $i = 0, 1, 2, \dots, N+1$ ) extends from one solar radius ( $1 R_\odot$ ) to one astronomical unit ( $1 \text{ AU}$ ). For a suitable computational time, we set the number of grids to  $N = 2000$ .

### 5.1. Initial and Boundary Conditions

We choose the following initial conditions (at  $t = 0$ ) (Chandran et al. 2011) for all grid points from  $r_0$  to  $r_{N+1}$  as

$$\begin{aligned} n &= n_\odot U_0 a_\odot / (U a), & U_0 &= U(r_0), \\ T_{\perp e} &= T_{\parallel e} = T_{\perp p} = T_{\parallel p} = T_\odot (3 - 2R_\odot/r)(r/R_\odot)^{-2/7}, \\ U &= (655 \text{ km/s})(1 + 20(R_\odot/r)^3)^{-1}, \\ E_W &= nm_p(\delta v_\odot)^2, \\ q_{\perp p} &= q_{\parallel p} = q_{\perp e} = q_{\parallel e} = 0. \end{aligned}$$

We use the boundary conditions at  $r_0$  close to the Sun (Chandran et al. 2011),

$$\begin{aligned} n &= n_\odot = 10^8 \text{ cm}^{-3}, \\ T_{\parallel e} &= T_{\perp e} = T_{\parallel p} = T_{\perp p} = T_\odot = 7 \times 10^5 \text{ K}, \\ E_W &= n_\odot m_p(\delta v_\odot)^2, & \delta v_\odot &= 41.4 \text{ km/s}. \end{aligned}$$

The rest value of the quantities ( $q_{\parallel e}, q_{\perp e}, q_{\parallel p}, q_{\perp p}, U$ ) at  $r_0$  is linearly extrapolated from their values in the next two grid points ( $r_1$  and  $r_2$ ). Also, the open boundary condition at  $r_{N+1}$  is applied.

## 6. NUMERICAL RESULTS

Here, we study the time and space evolution of the fast solar wind quantities ( $n, U, T_{\perp p}, T_{\parallel p}, T_{\perp e}, T_{\parallel e}, q_{\perp p}, q_{\parallel p}, q_{\perp e}, q_{\parallel e}, E_W$ ) by applying the two-fluid model in the kinetic theory framework.

Using the Bi-Maxwellian distribution function for protons and Kappa-Maxwellian distribution for electrons, the 11 coupled equations are derived. The numerical solution of the 11 coupled equations for different  $\kappa$  index ( $\kappa=2, 5, 7, 30$ ) is studied.

Figure 2 represents spatial variations of the electron and proton number densities (assumed to be equal,  $n_e = n_p = n$ ) from the Sun to the near Earth. The number density decreases approximately

from  $10^8 \text{ cm}^{-3}$  close the Sun to 1.67, 1.86, 2.16, and  $2.61 \text{ cm}^{-3}$  in near the Earth environment for  $\kappa=2, 5, 7$ , and 30, respectively. Near the Earth, the density increases with increasing  $\kappa$  index. For high  $\kappa$  index, the number density is in good agreement with observations recorded by *Ulysses* and previous studies (e.g., [Chandran et al. 2011](#)).

Close to the Sun, the density is comparable to the observed data near the solar minimum ([Allen & Cox \(2000\)](#), Table 14.19 therein). Power-law functions,  $n(r) \sim r^{-\alpha}$ , with the exponents  $\alpha \approx (2.224\%, 2.194\%, 2.154\%, \text{ and } 2.04\%) \pm 0.04\%$  are fitted to the number density at (0.3 - 1) AU for  $\kappa = 2, 5, 7$ , and 30 at (0.3 - 1) AU from the Sun.

Figure 3 shows the profiles of the fast solar wind speed  $U$  and the Alfvén speed  $V_A$  for different  $\kappa$  indices. Close to the Sun, outflow and Alfvén velocities decrease with decreasing  $\kappa$ . Expectedly, for large  $\kappa$  the results are in agreement with the Maxwellian model for electrons ([Chandran et al. 2011](#)). The position of the Alfvén critical point (at this point the outflow velocity reaches the Alfvén velocity) is obtained as  $r_A/R_\odot = 8.5, 8.4, 8.33$ , and 8.31 for  $\kappa = 2, 5, 7$ , and 30, respectively. We obtain the  $U(r_A) = 601.45, 615.55, 619.18$ , and 617.47 km/s, respectively. The outflow velocities are obtained as  $U(r_{AU}) \approx 822.85, 816.38, 806.36$ , and 804.63 km/s near the Earth environment. The simulated Alfvén velocity near the Earth is in agreement with the observational values ranging from 4.2 to 160.5 km/s at (0.3 - 0.7) AU ([Marsch et al. 1982](#)).

The parallel and perpendicular components of both proton and electron temperatures are demonstrated in Figures 4, and 5, respectively. It is clearly shown that the proton temperature in each direction increases with increasing  $\kappa$  index. From the Sun to about  $r \approx 26R_\odot$  the  $T_{\perp p}$  is significantly more than  $T_{\parallel p}$  for all  $\kappa$ . In region  $26 < r/R_\odot < 36$  the parallel temperature rises above the perpendicular component, which, is in agreement with [Chandran et al. \(2011\)](#).

Close to the Sun, the two components of electron temperatures are approximately the same. For small  $\kappa$  the high million kelvin temperatures for electrons are in good agreement with both observations and a previous study (e.g., [Zouganelis et al. 2004](#)) at the solar atmosphere. Expectedly, close the Sun the Maxwellian behavior for electrons is obtained for large  $\kappa$  (e.g., [Chandran et al.](#)

2011). The difference between the two components of the temperatures increases after about  $r/R_\odot \approx 3.92, 4.06, 4.25$ , and  $4.7$  for  $\kappa = 2, 5, 7$ , and  $30$ , respectively.

Observations show that  $T_{\parallel e}/T_{\perp e}$  tends to  $1.2$  in near the Earth environment, (e.g., [Feldman et al. 1975](#); [Pilipp et al. 1987](#); [Štverák et al. 2008](#)). We find this ratio to be about  $T_{\parallel e}/T_{\perp e} = 1.1, 1.06, 1.05$ , and  $1.02$  for  $\kappa = 2, 5, 7$ , and  $30$ , respectively, at  $1$  AU from the Sun. For both components, the exponents of the fitted power-law functions ( $T \approx r^{-\alpha}$ ) at a distance ( $0.3 - 1$ ) AU are shown in Figure 5.

Figure 6 shows the heating rate ratio (the ratio of the turbulent heating rate to the total heating rate) for both components of the electrons ( $Q_{\parallel e}/Q, Q_{\perp e}/Q$ ) and protons ( $Q_{\parallel p}/Q, Q_{\perp p}/Q$ ), and the total heating rate for electrons ( $Q_e/Q$ ) for different  $\kappa$  indices. The curves present the behavior of the energy exchanges between the shear Alfvén wave (and/or KAW) and the particles. As shown in the figure, close the Sun most of the wave-dissipated energy is absorbed by electrons in the parallel direction. Also, the absorbed energy increases with decreasing  $\kappa$  index. The absorbed energy by protons ( $Q_{\parallel p}/Q, Q_{\perp p}/Q$ ) and electrons ( $Q_{\perp e}/Q$ ) increases with increasing distance from the Sun ( $r$ ). Expectedly, for large  $\kappa$  index, both components of proton heating rates and the total heating rate for electrons are in good agreement with the previous study (e.g. [Chandran et al. 2011](#)). It is shown that the total turbulent heating rates ( $Q_{\parallel e}/Q + Q_{\perp e}/Q + Q_{\parallel p}/Q + Q_{\perp p}/Q$ ) approaches the unity.

The behaviors of the heat flux components (parallel and perpendicular) for both protons and electrons are represented in Figures 7, and 8, respectively. Both components of the proton heat flux decrease with decreasing  $\kappa$ . Near the Earth, the parallel component of proton heat flux is larger than the perpendicular component for all  $\kappa$ . The free-streaming heat flux for proton is given by (Equation 59),

$$q_{\text{fs},p} = 1.5nk_B T_p v_{\text{tp}}, \quad (59)$$

where  $v_{\text{tp}} = \sqrt{k_B T_p / m_p}$ . As we see in the figure,  $q_{\text{fs},p}$  decreases with decreasing  $\kappa$ . It is clearly shown that  $q_{\perp p}$  and  $q_{\parallel p}$  are smaller than free-streaming heat flux from the Sun to near the Earth.

The perpendicular and parallel component of the electron heat flux increase with decreasing  $\kappa$ . Generally, the electron heat flux in the perpendicular direction is significantly more than the parallel one for all  $\kappa$ . Also, close to the Sun, the total electron heat flux ( $q_e = \frac{2q_{\perp e} + q_{\parallel e}}{3}$ ) is approximately equal to the Spitzer approximation (Spitzer Jr & Härm 1953),

$$q_{\text{sh}} = -\kappa_{e0} T_e^{5/2} \frac{\partial T_e}{\partial r}, \quad (60)$$

where  $\kappa_{e0} = \frac{1.84 \times 10^{-5}}{\ln \Lambda} \text{ erg s}^{-1} \text{ K}^{-7/2} \text{ cm}^{-1}$ , and  $\ln \Lambda$  is the Coulomb logarithm. Near the Earth, the electron heat flux tends to the electron free-streaming heat flux as

$$q_{\text{fs,e}} = 1.5 n k_B T_e v_{\text{te}}, \quad (61)$$

where  $v_{\text{te}} = \sqrt{k_B T_e / m_e}$ , and is comparable with *Helios* data for electron heat flux at 1 AU (Le Chat et al. 2012). A considerable difference between the parallel and perpendicular components of electron heat flux may be related to the wave-particle interactions in plasma (Figure 6) and also the non-Maxwellian distribution for electrons. According to Figure 6, the absorbed energy of electrons (in wave-particle interactions) decreases in the parallel direction but increases in the perpendicular direction from the Sun to Earth. Another factor affecting this difference may be related to transporting the electron energy from the parallel to the perpendicular direction (Štverák et al. 2015). The power exponents  $\alpha_{\perp}$ ,  $\alpha_{\parallel}$  for the power-law function fitted to the fluxes at (0.3 - 1) AU are presented in Figure 8. The value of the electron and proton heat fluxes, temperatures, and solar wind energy fluxes for various  $\kappa$  indices at 1 AU are listed in Table 1.

**Table 1.** The Components of Heat Flux for Electrons and Protons, the Components of Temperature for Electrons and Protons, and the Total Energy Flux for Different  $\kappa$  (at 1 AU) Are Tabulated.

$\kappa$ Index	2	5	7	30
$q_{\parallel e}(\text{W/m}^2)$	$8.3 \times 10^{-13}$	$5.86 \times 10^{-13}$	$4.45 \times 10^{-13}$	$3.3 \times 10^{-13}$
$q_{\perp e}(\text{W/m}^2)$	$1.12 \times 10^{-5}$	$8.3 \times 10^{-6}$	$7.5 \times 10^{-6}$	$6.99 \times 10^{-6}$
$q_{\parallel p}(\text{W/m}^2)$	$7.83 \times 10^{-11}$	$8.01 \times 10^{-11}$	$8.3 \times 10^{-11}$	$8.7 \times 10^{-11}$
$q_{\perp p}(\text{W/m}^2)$	$2.19 \times 10^{-11}$	$3.14 \times 10^{-11}$	$3.5 \times 10^{-11}$	$4.1 \times 10^{-11}$
$T_{\parallel e}(\text{K})$	$1.64 \times 10^5$	$1.32 \times 10^5$	$1.09 \times 10^5$	$9.32 \times 10^4$
$T_{\perp e}(\text{K})$	$1.54 \times 10^5$	$1.25 \times 10^5$	$1.01 \times 10^5$	$9.14 \times 10^4$
$T_{\parallel p}(\text{K})$	$1.6 \times 10^5$	$1.7 \times 10^5$	$1.8 \times 10^5$	$1.9 \times 10^5$
$T_{\perp p}(\text{K})$	$1.16 \times 10^5$	$1.37 \times 10^5$	$1.52 \times 10^5$	$1.6 \times 10^5$
$F_{\text{tot}}(\text{W/m}^2)$	$7.8 \times 10^{-4}$	$8.5 \times 10^{-4}$	$9.5 \times 10^{-4}$	$1.1 \times 10^{-3}$

## 7. CONCLUSION

Electrons and protons are the main components of the solar wind, so the two-fluid model in the presence of some kinetic effects is useful to study the characteristics of the system. Observational proofs, such as the anisotropic behavior of the temperature of the solar wind electrons, show that the electrons distribution deviates from the well-known Maxwellian distribution.

In this paper, we provided a two-fluid model for the solar wind consisting of the Bi-Maxwellian distribution for protons and the Kappa-Maxwellian distribution for electrons. As the Kappa distribution function might tend to the Maxwellian in the limit of the large  $\kappa$  index, the small  $\kappa$  (less than 5) showed more deviation from the Maxwellian.

We derived 11 coupled equations for fast solar wind model quantities, namely  $n, U, T_{\perp p}, T_{\parallel p}, T_{\perp e}, T_{\parallel e}, q_{\perp p}, q_{\parallel p}, q_{\perp e}, q_{\parallel e}, E_W$ . To this end, we calculated the velocity space moments up to the fourth order. The functional forms of the six equations (Equations 23, 27, 28, 31-33) have the same form seen in Chandran et al. (2011), which was derived for the Bi-Maxwellian protons. We also presented five new equations (Equations 24-26, 29, and 30) in the presence of the Kappa-Maxwellian distribution for electrons. The  $\kappa$  changing from 1.5 to infinity is a characteristic of the Kappa distribution and is considered as a free parameter for the present model.

We showed that in the limit of the large  $\kappa$ , the equation for electron parallel heat flux (Equation 28) behaves like the equation for the proton parallel heat flux (Equation 26), which derived in the presence of the Maxwellian distribution for electrons. We also used the Landau damping model for the exchange of energies between the particles and waves (shear Alfvén wave).

Applying the initial and boundary conditions, and the ICN numerical method, the set of equations were solved. The main results are as follows:

1. Expectedly, the number density  $n(r)$  (assumed to be equal for electrons and protons) shows the scale-free behavior and decreases with increasing the distance from the Sun. The power-law exponent ( $\alpha$ ) for the density at (0.3 - 1) AU was obtained as  $\sim 2.0 - 2.3$  for different  $\kappa$ , which is in agreement with observations recorded by *Helios* (Štverák et al. 2015). This power-law behavior may be related to the nature of the Kappa distribution. The power-law behavior

for the number density was reported in the literature (e.g., [Erickson 1964](#); [Allen & Cox 2000](#); [Štverák et al. 2015](#)). Also, near the Earth, the number density decreases with decreasing  $\kappa$  index.

2. The outflow speed increases with increasing distance from the Sun ( $r$ ), while the Alfvén velocity decreases with  $r$ . For small  $\kappa$  index, the Alfvénic critical point occurs at a distance close to the Sun. It seems the solution for solar wind flow is analogous to the properties of plasma flow in the Alfvénic black hole. An Alfvénic black hole may be created using a magnetic flux tube with a variable cross section and super-Alfvénic flow. Using the linearized MHD equations in the presence of super-Alfvénic plasma flow, a tensorial form of the Alfvén waves (with an accompanying metric) was obtained ([Gheibi et al. 2018](#)). The resultant metric is singular at a point (horizon of black hole) where the local Alfvén speed is equal to flow speed. The horizon of the Alfvénic black hole is likely similar to the critical Alfvénic point in the solar wind solution. In the solar wind solution, from the lower solar atmosphere (lower corona) the flow starts to accelerate (with considerable acceleration  $dU/dr > 0$ ) and at the critical Alfvénic point (like to the horizon of the Alfvénic black hole), the flow speed equals to the Alfvénic speed and continuous to very slightly accelerate and approach approximately constant speed far from the Sun as the flux tube diverges. Close to the Sun, the fast solar wind propagates with low speeds for small  $\kappa$  (Figure 2). But near the Earth, high speed is related to the small  $\kappa$ . We found the outflow speed is in the range of 804-822 km/s (near the Earth) and satisfies with the observational data ([Bame et al. 1993](#); [Feldman et al. 2005](#)). Expectedly, for large  $\kappa$ , the value of the outflow speed is in good agreement with [Chandran et al. \(2011\)](#), who they used a Maxwellian distribution for electrons.
3. Close to the Sun and for  $\kappa$  around 7, the proton temperature is in consistent with the observational value (Figure 4). This is also in agreement with [Pierrard et al. \(2016\)](#), who modeled the electrons close to the Sun. The parallel and perpendicular components of the electron temperature for  $\kappa=7$  are also comparable with observations. Getting away from the Sun, small

$\kappa$  shows temperatures of several million kelvin for electrons (Zouganelis et al. 2004). This high temperature is related to the extraordinary nature of the solar atmosphere (corona). Near the Earth and for small  $\kappa$ , the value of the electron temperature ratio ( $T_{\parallel e}/T_{\perp e}$ ) was obtained as about 1.1, which is in agreement with observations (Štverák et al. 2008).

4. The perpendicular and parallel heat flux components of electrons increase with decreasing  $\kappa$  index. The electron heat flux approximately is comparable with the free-streaming analytical curve (collisionless regime) near the Earth and the Spitzer-Härm solution (Collisional regime) near the Sun.

Finally, this study shows that while some of the observational quantities (e.g., electron and proton temperature) are well modeled with  $\kappa=7$  close to the Sun and far away from the Sun (near the Earth), other quantities (e.g., the temperature ratio for electrons) are satisfied with a small  $\kappa$  index (less than 5). Thus, this study encourages us to develop the multi-index models including three or more  $\kappa$  indices (large  $\kappa$  close the Sun and small near the Earth) for the fast solar wind.



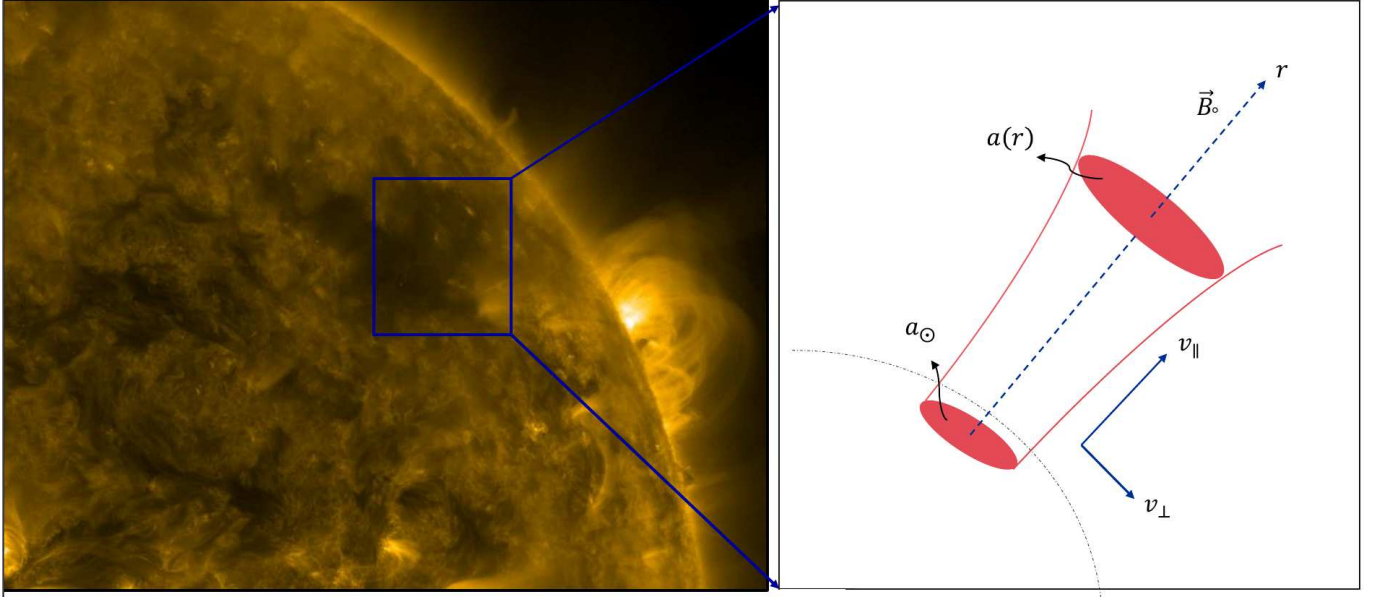


**Figure 1.** Left: an image at  $171 \text{ \AA}$  observed by the *SolarDynamic Observatory*(*SDO*)/Atmospheric Imaging Assembly (AIA) on 2013:07:07. Right: a schematic representation of an open magnetic flux tube on the Sun. The parameters  $a_{\odot}$  and  $a(r)$  are the cross section of the flux tube on the photosphere and at a distance  $r$  from the Sun, respectively.

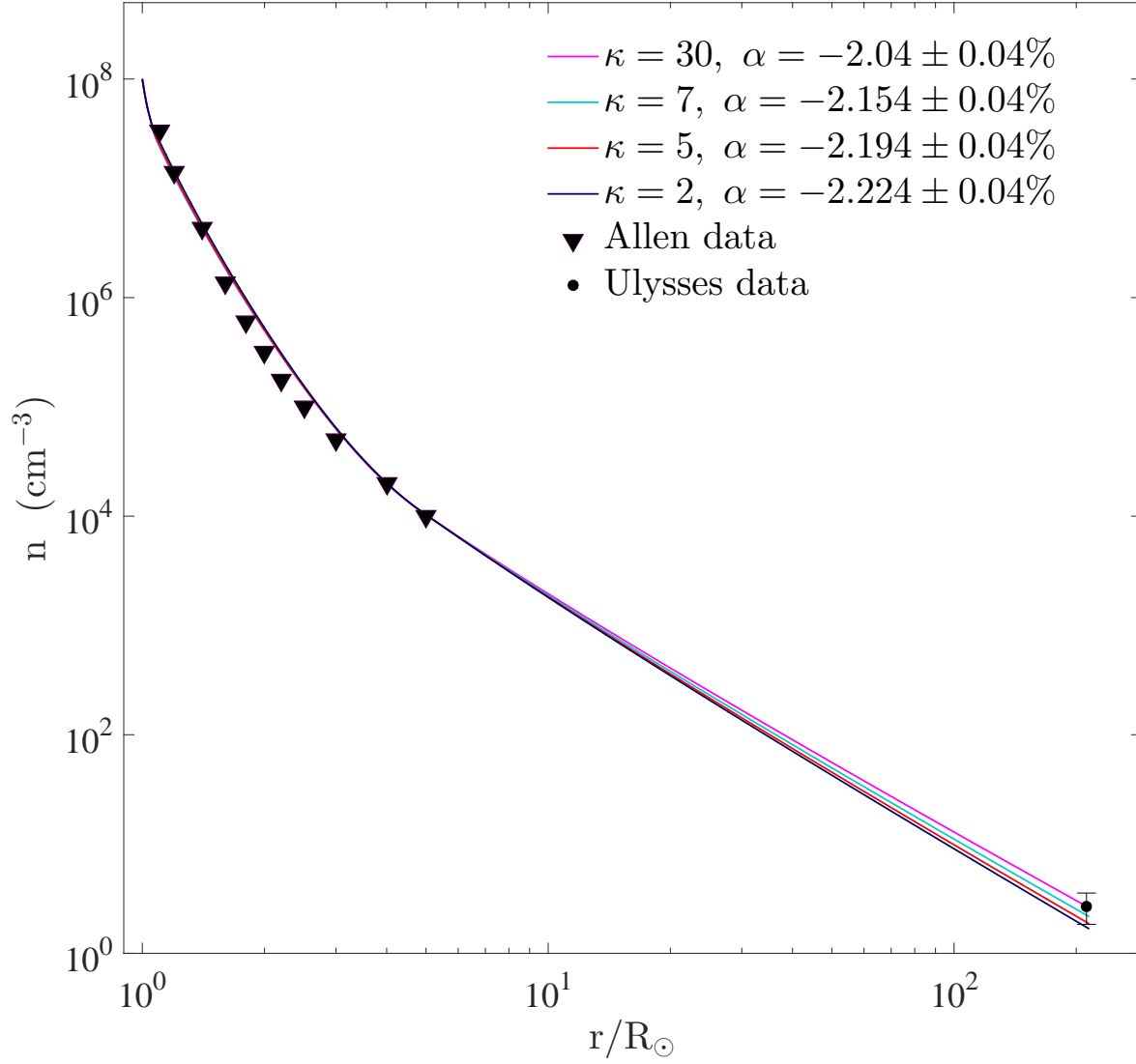


**Figure 2.** Number density for  $\kappa = 2, 5, 7$ , and  $30$  vs the distances ( $r/R_{\odot}$ ). The filled circle ( $\bullet$ ) is mean proton density measured by *Ulysses* at its first orbit (McComas et al. 2000). The ( $\blacktriangledown$ s) show the polar coronal hole observed data near the solar minimum (Allen & Cox 2000). The exponent of the fitted power-law function to the density at (0.3 - 1) AU is presented for all  $\kappa$ .

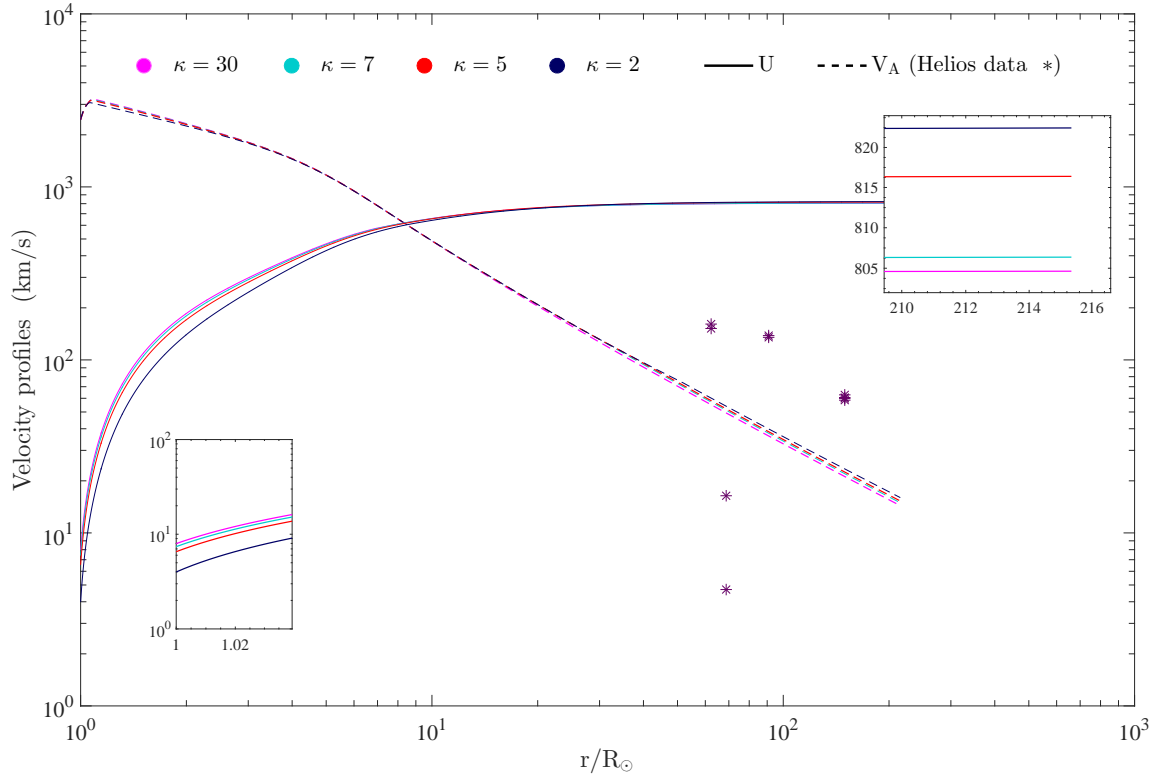


**Figure 3.** The solid lines are solar wind outflow velocities and the dashed lines are the Alfvén velocities for  $\kappa = 2, 5, 7$ , and  $30$  from the Sun to near the Earth. The (*\*s*) show the *Helios* data reported for the fast solar wind (Marsch et al. 1982). The inset box shows the dependency of the velocities on the  $\kappa$  index close to the Sun and near the Earth.

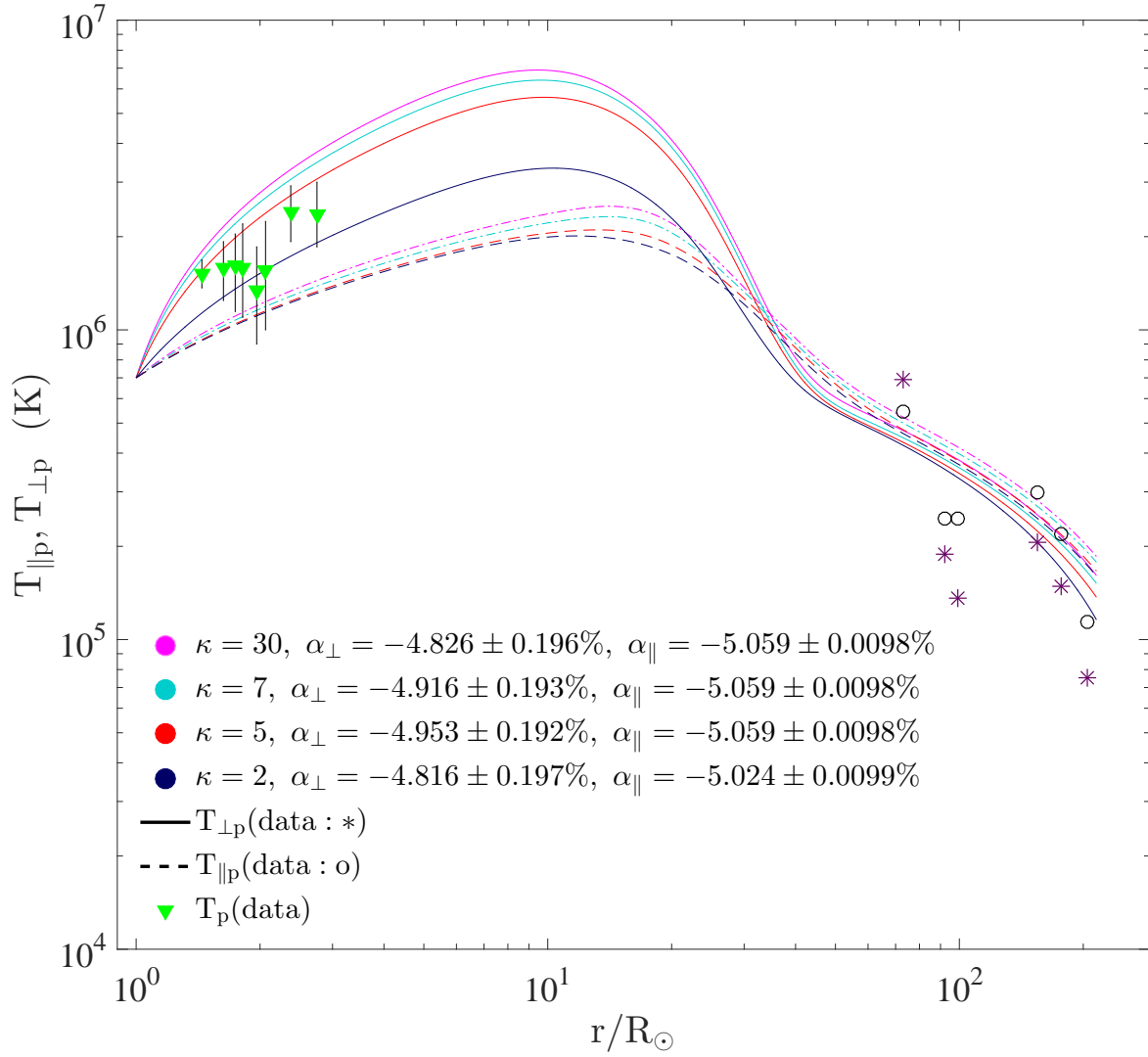


**Figure 4.** The solid lines represent the perpendicular temperature and the dashed lines represent the parallel temperature for protons for  $\kappa = 2, 5, 7$ , and  $30$  vs the distance from the Sun. The ( $*$ s) and ( $o$ s) show the *Helios* data reported for parallel and perpendicular temperatures for the fast solar wind, respectively (Marsch et al. 1982), the ( $\blacktriangledown$ s) show the UVCS/*SoHO* data for the proton temperature, the power-law indices ( $\alpha_{\perp}, \alpha_{\parallel}$ ) for all  $\kappa$  are presented.

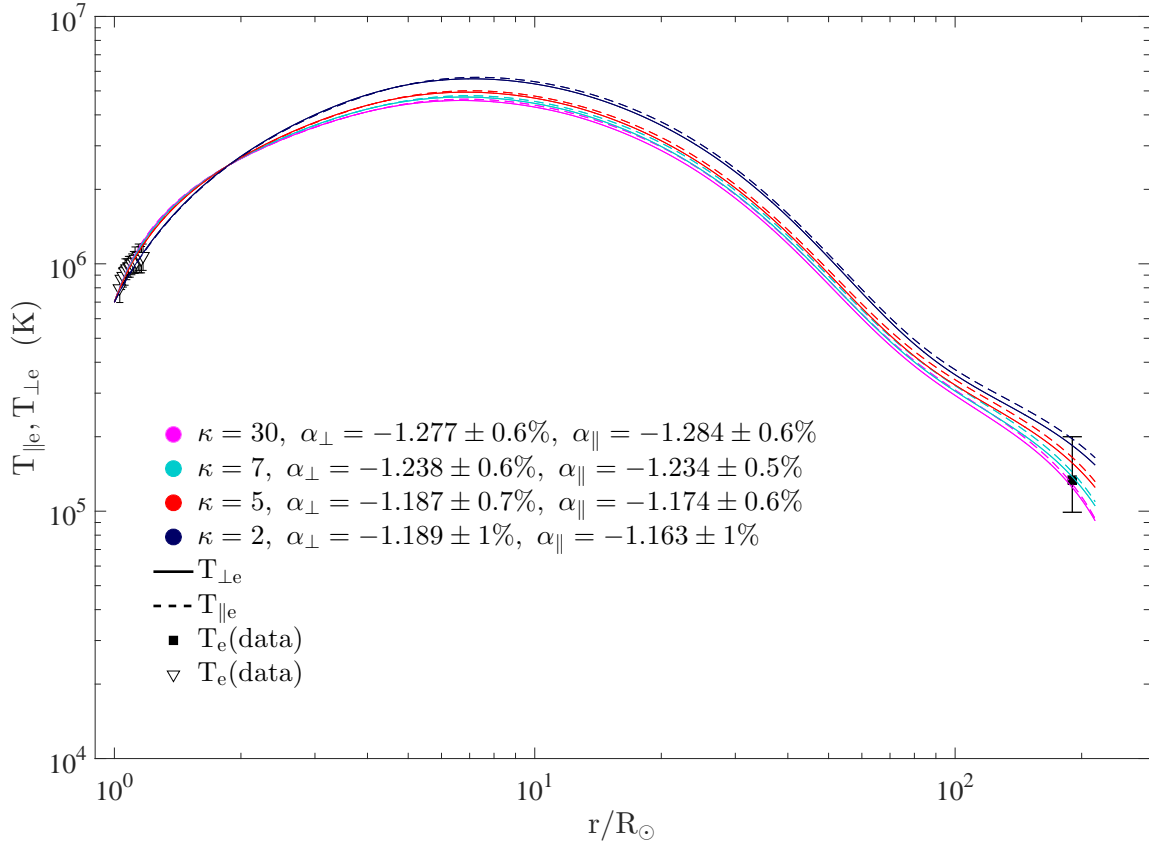


**Figure 5.** The solid lines are perpendicular temperature and the dashed lines are the parallel temperature for electrons for  $\kappa = 2, 5, 7$ , and  $30$  from the Sun to the Earth. The ( $\nabla$ s) show the *SoHO*/SUMER data of electron temperature in a polar coronal hole (Landi 2008) and the square ( $\blacksquare$ ) is the mean electron temperature for the fast solar wind that measured by ISEE 3 and *Ulysses* Newbury et al. (1998).  $\alpha_\perp$  and  $\alpha_\parallel$  are the power-law indices for  $\kappa = 2, 5, 7$ , and  $30$  at  $(0.3 - 1)$  AU.

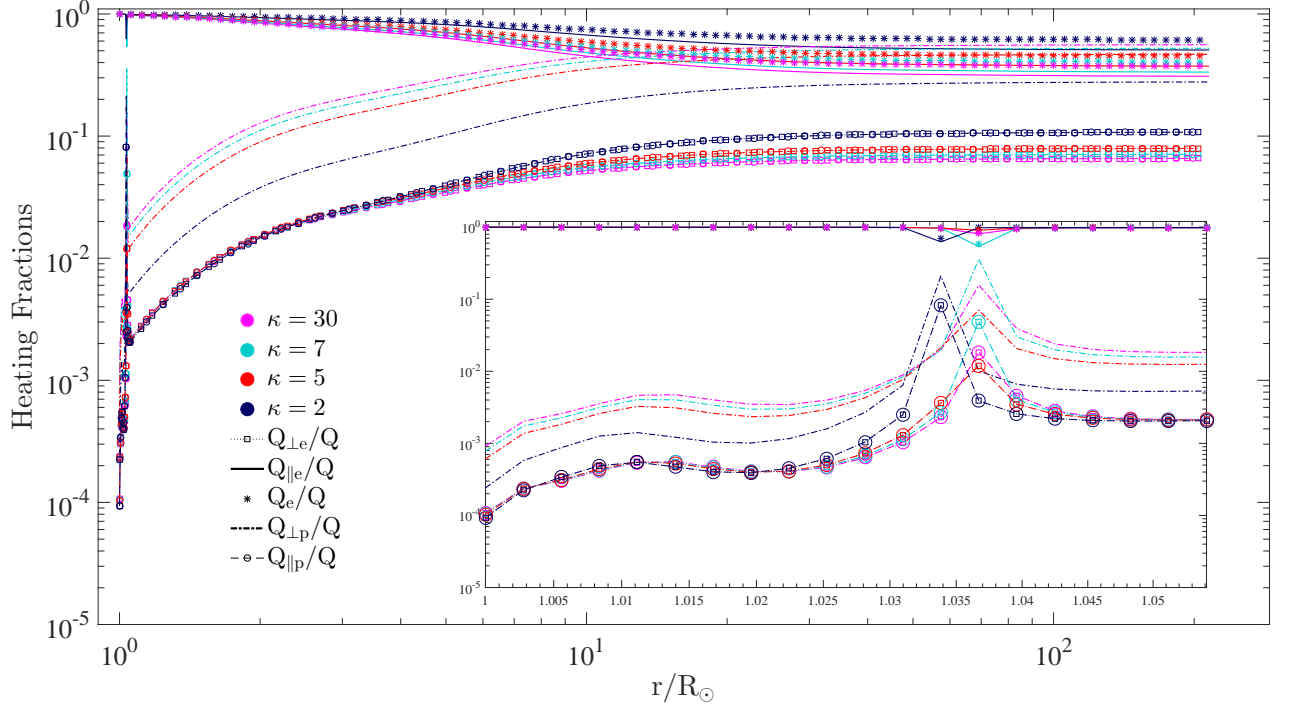


**Figure 6.** Ratio of the turbulence heating rates of electrons and protons ( $\parallel, \perp$ ) and total heating rate for electrons for  $\kappa = 2, 5, 7$ , and  $30$ . The inset box shows the variability of the mentioned parameters close to the Sun.

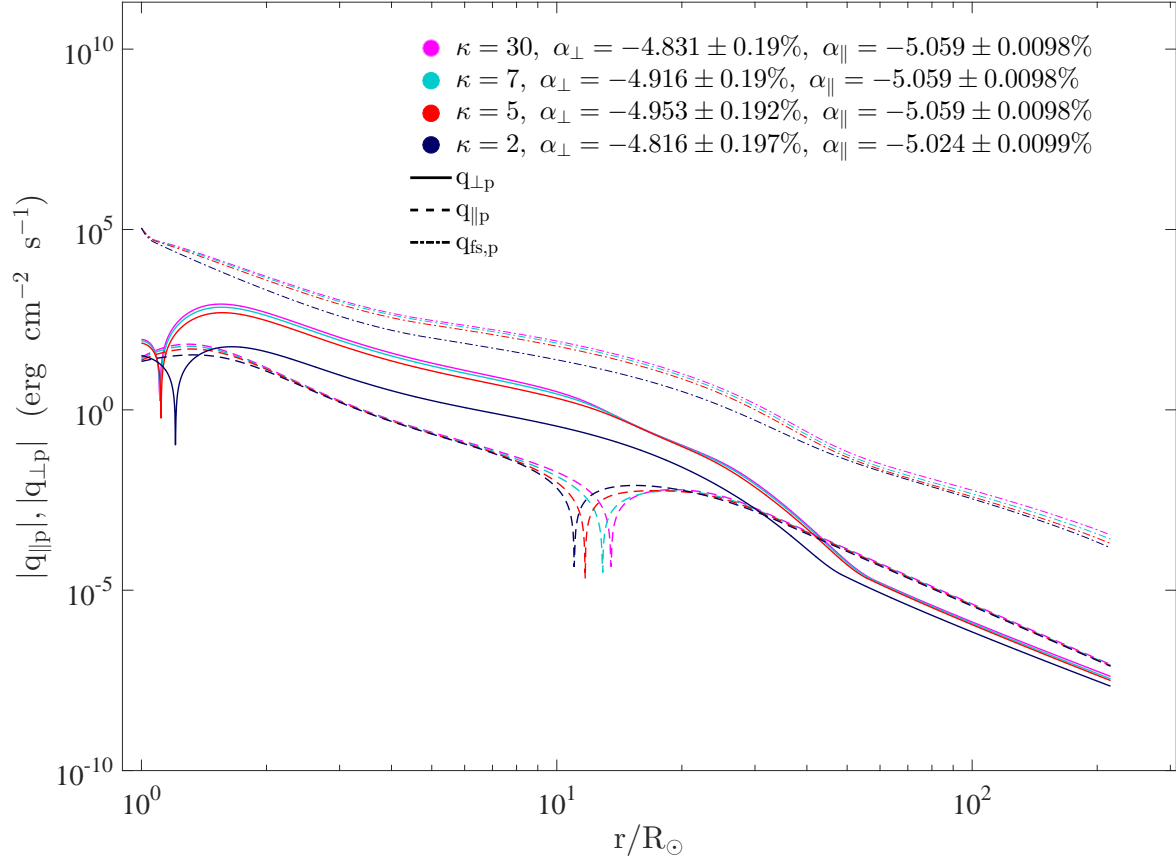


**Figure 7.** The perpendicular heat flux ( $q_{\perp,p}$ ), the parallel heat flux ( $q_{\parallel,p}$ ), and the free-streaming analytical calculation ( $q_{\text{fs},p}$ ) of the protons are presented. The power-law indices ( $\alpha_{\perp}, \alpha_{\parallel}$ ) for different  $\kappa$  are presented.

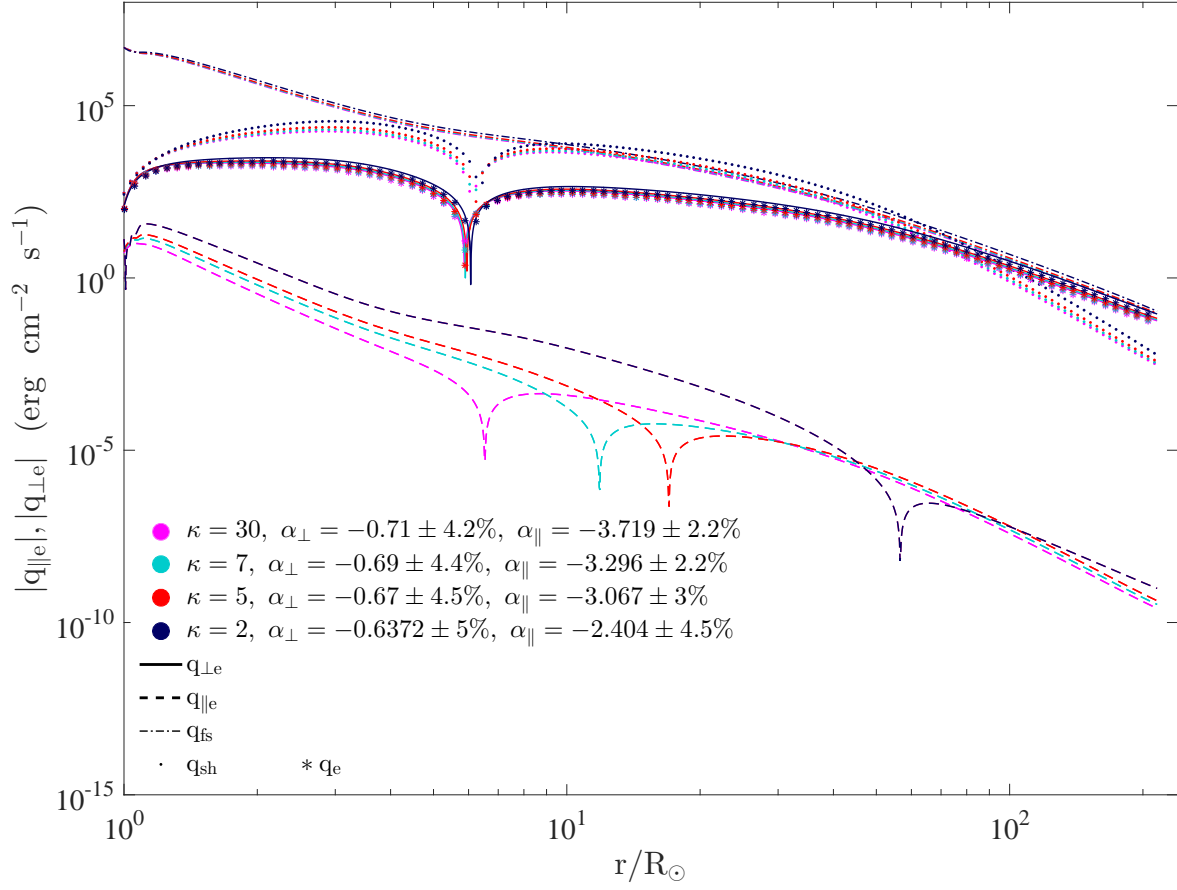


**Figure 8.** The perpendicular heat flux  $q_{\perp e}$ , the parallel heat flux  $q_{\parallel e}$ , the free-streaming analytical calculation  $q_{fs,e}$ , the Spitzer-Härm  $q_{sh}$  heat flux, and the total heat flux  $q_e = \frac{2q_{\perp e} + q_{\parallel e}}{3}$  for the electrons are presented. The power-law exponents for the heat fluxes at (0.3 - 1) AU are obtained.



## ACKNOWLEDGEMENT

The authors would like to thank the *Helios* team for the solar wind data. We also thank Dr. Danial Verscharen University College London-Mullard Space Science Laboratory for his very helpful discussion. We would like to give a special thanks to Professor Stefaan Poedts for his suggestion regarding the idea of the effects of Kappa distribution for electrons in a two-fluid model for solar winds. We also gratefully thank the anonymous referee for very helpful and constructive comments and suggestions that improved the manuscript. The authors would like to express their gratitude to the Iran National Science Foundation (INSF) for supporting this research under grant No. 93043701. We acknowledge the support from the High Performance Computing Center of Department of physics, University of Zanjan.

## REFERENCES

- |   |   |
|---|---|
| <p>Alfvén, H., &amp; Lindblad, B. 1947, Monthly Notices of the Royal Astronomical Society, 107, 211</p> <p>Alipour, N., Mohammadi, F., &amp; Safari, H. 2019, The Astrophysical Journal Supplement Series, 243, 20</p> <p>Allen, C. W., &amp; Cox, A. N. 2000, Allen's astrophysical quantities (4th ed.;New York: Springer)</p> <p>Amagishi, Y. 1986, Physical review letters, 57, 2807</p> <p>Bale, S., Kasper, J., Howes, G., et al. 2009, Physical review letters, 103, 211101</p> <p>Bame, S., Goldstein, B., Gosling, J., et al. 1993, Geophysical research letters, 20, 2323</p> <p>Basu, B. 2009, Physics of Plasmas, 16, 052106</p> <p>Bittencourt, J. A. 2004, Fundamentals of Plasma Physics (Springer-Verlag)</p> | <p>Borovsky, J. E., &amp; Funsten, H. O. 2003, Journal of Geophysical Research (Space Physics), 108, 1246</p> <p>Bruno, R., &amp; Carbone, V. 2005, Living Reviews in Solar Physics, 2, 4</p> <p>Cattaert, T., Hellberg, M. A., &amp; Mace, R. L. 2007, Physics of Plasmas, 14, 082111</p> <p>Chandran, B. D. G. 2018, Journal of Plasma Physics, 84, 905840106</p> <p>Chandran, B. D. G., Dennis, T. J., Quataert, E., &amp; Bale, S. D. 2011, ApJ, 743, 197</p> <p>Chané, E., Raeder, J., Saur, J., et al. 2015, Journal of Geophysical Research: Space Physics, 120, 8517</p> <p>Chapman, S. 1929, MNRAS, 89, 456</p> <p>Chappell, C. R., Moore, T. E., &amp; Waite, Jr., J. H. 1987, J. Geophys. Res., 92, 5896</p> |
|---|---|

- Chen, C., Horbury, T., Schekochihin, A., et al. 2010, *Physical review letters*, 104, 255002
- Cho, J., & Vishniac, E. T. 2000, *ApJ*, 539, 273
- Coleman, Jr., P. J. 1968, *ApJ*, 153, 371
- Cramer, N. F. 2011, *The physics of Alfvén waves* (John Wiley & Sons)
- Cranmer, S. R., Gibson, S. E., & Riley, P. 2017, *SSRv*, 212, 1345
- Demars, H., & Schunk, R. 1990, *Planetary and Space Science*, 38, 1091
- Demars, H. G., & Schunk, R. W. 1991, *Planet. Space Sci.*, 39, 435
- Dewar, R. L. 1970, *Physics of Fluids*, 13, 2710
- Durney, B. 1971, *ApJ*, 166, 669
- Durney, B. R., & Roberts, P. H. 1971, *ApJ*, 170, 319
- Erickson, W. C. 1964, *ApJ*, 139, 1290
- Esmaili, S., Nasiri, M., Dadashi, N., & Safari, H. 2016, *Journal of Geophysical Research (Space Physics)*, 121, 9340
- Farhang, N., Safari, H., & Wheatland, M. S. 2018, *The Astrophysical Journal*, 859, 41
- Feldman, U., Landi, E., & Schwadron, N. A. 2005, *Journal of Geophysical Research (Space Physics)*, 110, A07109
- Feldman, W. C., Asbridge, J. R., Bame, S. J., Montgomery, M. D., & Gary, S. P. 1975, *J. Geophys. Res.*, 80, 4181
- Frank, L. A. 1971, *J. Geophys. Res.*, 76, 5202
- Gary, S. P., & Karimabadi, H. 2006, *Journal of Geophysical Research (Space Physics)*, 111, A11224
- Gary, S. P., & Wang, J. 1996, *Journal of Geophysical Research: Space Physics*, 101, 10749
- Geiss, J., Gloeckler, G., & von Steiger, R. 1995, *SSRv*, 72, 49
- Gershman, D. J., Adolfo, F., Dorelli, J. C., et al. 2017, *Nature communications*, 8, 14719
- Gheibi, A., Safari, H., & Innes, D. E. 2018, *European Physical Journal C*, 78, 662
- Goedbloed, J. H., Goedbloed, J., & Poedts, S. 2004, *Principles of magnetohydrodynamics: with applications to laboratory and astrophysical plasmas* (Cambridge university press)
- Goldreich, P., & Sridhar, S. 1995, *ApJ*, 438, 763
- Gosling, J. T., McComas, D. J., Phillips, J. L., & Bame, S. J. 1991, *J. Geophys. Res.*, 96, 7831
- Gray, L. J., Beer, J., Geller, M., et al. 2010, *Reviews of Geophysics*, 48, RG4001
- Hartle, R. E., & Sturrock, P. A. 1968, *ApJ*, 151, 1155
- Hellinger, P., Trávníček, P., Kasper, J. C., & Lazarus, A. J. 2006, *Geophys. Res. Lett.*, 33, L09101
- Hollweg, J. V. 1981, *Solar Physics*, 70, 25
- Howes, G. G. 2008, *Physics of Plasmas*, 15, 055904
- . 2015, *Kinetic Turbulence*, ed. A. Lazarian, E. M. de Gouveia Dal Pino, & C. Melioli (Berlin, Heidelberg: Springer Berlin Heidelberg), 123–152
- Howes, G. G., TenBarge, J. M., Dorland, W., et al. 2011, *Physical review letters*, 107, 035004

- Hu, Y. Q., Esser, R., & Habbal, S. R. 1997, *J. Geophys. Res.*, 102, 14661
- Jiang, Y. W., Liu, S., & Petrosian, V. 2009, *The Astrophysical Journal*, 698, 163
- Kalman, G., Montes, C., & Quémada, D. 1968, *The Physics of Fluids*, 11, 1797
- Kasper, J. C., Lazarus, A. J., & Gary, S. P. 2002, *Geophysical research letters*, 29, 20
- Kasper, J. C., Lazarus, A. J., Steinberg, J. T., Ogilvie, K. W., & Szabo, A. 2006, *Journal of Geophysical Research (Space Physics)*, 111, A03105
- Kopp, R. A., & Holzer, T. E. 1976, *SoPh*, 49, 43
- Kulsrud, R. M. 1983, *Handbook of plasma physics*, 1, 115
- Landi, E. 2008, *ApJ*, 685, 1270
- Le Chat, G., Issautier, K., & Meyer-Vernet, N. 2012, *Solar Physics*, 279, 197
- Leiler, G., & Rezzolla, L. 2006, *PhRvD*, 73, 044001
- Lie-Svendsen, Ø., Leer, E., & Hansteen, V. H. 2001, *Journal of Geophysical Research: Space Physics*, 106, 8217
- Lin, R. P. 1980, *SoPh*, 67, 393
- Livadiotis, G. 2017, *Kappa distributions: theory and applications in plasmas* (Elsevier)
- Livadiotis, G., & McComas, D. 2013, *Space Science Reviews*, 175, 183
- Lysak, R. L., & Lotko, W. 1996, *J. Geophys. Res.*, 101, 5085
- Maron, J., & Goldreich, P. 2001, *ApJ*, 554, 1175
- Marsch, E. 2006, *Living Reviews in Solar Physics*, 3, 1
- Marsch, E., Rosenbauer, H., Schwenn, R., Muehlhaeuser, K.-H., & Neubauer, F. M. 1982, *J. Geophys. Res.*, 87, 35
- McComas, D. J., Ebert, R. W., Elliott, H. A., et al. 2008, *Geophys. Res. Lett.*, 35, L18103
- McComas, D. J., Barraclough, B. L., Funsten, H. O., et al. 2000, *J. Geophys. Res.*, 105, 10419
- Meis, T., & Marcowitz, U. 2012, *Numerical solution of partial differential equations*, Vol. 32 (Springer)
- Meng, X., van der Holst, B., Tóth, G., & Gombosi, T. I. 2015, *MNRAS*, 454, 3697
- Meyer-Vernet, N. 2007, *Basics of the solar wind* (Cambridge University Press)
- Morton, R. J., Tomczyk, S., & Pinto, R. 2015, *Nature Communications*, 6, 7813
- Newbury, J., Russell, C., Phillips, J., & Gary, S. 1998, *Journal of Geophysical Research: Space Physics*, 103, 9553
- Olbert, S. 1968, in *Physics of the Magnetosphere* (Springer), 641–659
- Parker, E. 1958, *The Physics of Fluids*, 1, 171
- Parker, E. N. 1965, *SSRv*, 4, 666
- Perreault, P., & Akasofu, S.-I. 1978, *Geophysical Journal*, 54, 547
- Pierrard, V., & Lazar, M. 2010, *SoPh*, 267, 153
- Pierrard, V., Lazar, M., Poedts, S., et al. 2016, *SoPh*, 291, 2165
- Pierrard, V., Maksimovic, M., & Lemaire, J. 2001, *Ap&SS*, 277, 195
- Pilipp, W. G., Miggenrieder, H., Mühlhäuser, K.-H., et al. 1987, *J. Geophys. Res.*, 92, 1103

- Priest, E. 2014, *Magnetohydrodynamics of the Sun* (Cambridge University Press)
- Quataert, E. 1998, *ApJ*, 500, 978
- Qureshi, M. N. S., Sehar, S., & Shah, H. A. 2014, *Journal of Physics: Conference Series*, 516, 012013
- Raboonik, A., Safari, H., Alipour, N., & Wheatland, M. S. 2017, *ApJ*, 834, 11
- Recktenwald, G. W. 2004, *Mechanical Engineering*, 10, 1
- Roberts, D. A., Klein, L. W., Goldstein, M. L., & Matthaeus, W. H. 1987, *J. Geophys. Res.*, 92, 11021
- Roberts, P. H., & Soward, A. M. 1972, *Proceedings of the Royal Society of London Series A*, 328, 185
- Rudakov, L., Mithaiwala, M., Ganguli, G., & Crabtree, C. 2011, *Physics of Plasmas*, 18, 012307
- Salem, C. S., Howes, G. G., Sundkvist, D., et al. 2012, *ApJL*, 745, L9
- Schreiner, A., & Saur, J. 2017, *The Astrophysical Journal*, 835, 133
- Schunk, R. W. 1975, *Planet. Space Sci.*, 23, 437
- Shaaban, S. M., Lazar, M., Poedts, S., & Elhanbaly, A. 2017, *Ap&SS*, 362, 13
- Sharma, P., Hammett, G. W., Quataert, E., & Stone, J. M. 2006, *ApJ*, 637, 952
- Sharma, R. P., Goyal, R., Gaur, N., & Scime, E. E. 2016, *EPL (Europhysics Letters)*, 113, 25001
- Shoda, M., Yokoyama, T., & Suzuki, T. K. 2018a, *ApJ*, 853, 190
- . 2018b, *ApJ*, 860, 17
- Snyder, P. B., Hammett, G. W., & Dorland, W. 1997, *Physics of Plasmas*, 4, 3974
- Spitzer Jr, L., & Härm, R. 1953, *Physical Review*, 89, 977
- Stix, T. H. 1992, *Waves in plasmas* (New York: SpringerVerlag)
- Štverák, Š., Trávníček, P. M., & Hellinger, P. 2015, *Journal of Geophysical Research: Space Physics*, 120, 8177
- TenBarge, J. M., & Howes, G. G. 2012, *Physics of Plasmas*, 19, 055901
- TenBarge, J. M., Howes, G. G., & Dorland, W. 2013, *ApJ*, 774, 139
- Teukolsky, S. A. 2000, *PhRvD*, 61, 087501
- Thomas, J. W. 2013, *Numerical partial differential equations: finite difference methods*, Vol. 22 (Springer)
- Štverák, Š., Trávníček, P., Maksimovic, M., et al. 2008, *Journal of Geophysical Research (Space Physics)*, 113, A03103
- Vasyliunas, V. M. 1968, *Journal of Geophysical Research*, 73, 2839
- Vranjes, J., & Poedts, S. 2010, *The Astrophysical Journal*, 719, 1335
- Whang, Y. C., & Chang, C. C. 1965, *J. Geophys. Res.*, 70, 4175
- Wheatland, M. S. 2005, *PASA*, 22, 153

- Wu, D. J., Feng, H. Q., Li, B., & He, J. S. 2016, Journal of Geophysical Research (Space Physics), 121, 7349
- Young, D. T., Balsiger, H., & Geiss, J. 1982, J. Geophys. Res., 87, 9077
- Zhao, J., Wu, D., & Lu, J. 2011, The Astrophysical Journal, 735, 114
- Zouganelis, I., Maksimovic, M., Meyer-Vernet, N., Lamy, H., & Issautier, K. 2004, The Astrophysical Journal, 606, 542